Journal of Applied Biomechanics, (Ahead of Print)
https://doi.org/10.1123/jab.2020-0222

Human Kinetics
ORIGINAL RESEARCH

Estimating Center of Mass Kinematics During Perturbed Human Standing Using Accelerometers

Sandra K. Hnat,[1,2] Musa L. Audu,[1,2] Ronald J. Triolo,[1,2] and Roger D. Quinn[1]
[1]Case Western Reserve University; [2]Louis Stokes Cleveland VA Medical Center

Estimating center of mass (COM) through sensor measurements is done to maintain walking and standing stability with exoskeletons. The authors present a method for estimating COM kinematics through an artificial neural network, which was trained by minimizing the mean squared error between COM displacements measured by a gold-standard motion capture system and recorded acceleration signals from body-mounted accelerometers. A total of 5 able-bodied participants were destabilized during standing through: (1) unexpected perturbations caused by 4 linear actuators pulling on the waist and (2) volitionally moving weighted jars on a shelf. Each movement type was averaged across all participants. The algorithm's performance was quantified by the root mean square error and coefficient of determination (R^2) calculated from both the entire trial and during each perturbation type. Throughout the trials and movement types, the average coefficient of determination was 0.83, with 89% of the movements with $R^2 > .70$, while the average root mean square error ranged between 7.3% and 22.0%, corresponding to 0.5- and 0.94-cm error in both the coronal and sagittal planes. COM can be estimated in real time for balance control of exoskeletons for individuals with a spinal cord injury, and the procedure can be generalized for other gait studies.

Keywords: musculoskeletal biomechanics, rehabilitation, exoskeletons, balance, control

Spinal cord injuries (SCIs) resulting in lower limb paralysis can limit mobility and decrease quality of life.[1] The National SCI Statistical Center projects an incidence of approximately 17,730 new cases of SCI each year,[2,3] with a prevalence of 290,000 in the United States in 2020.[4] Powered orthoses, or exoskeletons, are an emerging field of research aiming to improve mobility for individuals with SCI.[5] These devices are worn in parallel to the user's lower body segments, where electric motors at the joints guide the affected limbs through walking, standing, and sitting motions.[6] Exoskeletons can improve muscle tone and strength in persons with incomplete SCI during rehabilitation and gait training.[7–11] Some commercial models have been marketed to generate walking movements in individuals with complete paraplegia, including Ekso (Ekso Bionics, Richmond, CA),[12] ReWalk (ReWalk Robotics, Yokneam, Israel),[13] and Indego (Parker Hannifin, Mayfield Heights, OH,).[14]

The phase-based controllers used in these commercial devices have been designed exclusively for stepping, where the electric motors follow predefined joint angle or torque trajectories characteristic of able-bodied walking.[15–18] These controllers are unable to stabilize the user and do not correct for unexpected disturbances such as tripping or volitional movements during activities of daily living.[19] Exoskeleton users stabilize themselves with upper limb effort on crutches or a walker, which contributes to an increase of metabolic expenditure.[20–22] Adding stabilizing controllers to powered exoskeletons would allow users to maintain balance, improve safety, and reduce energy cost during standing and walking.

Hnat, Audu, and Triolo are with the Department of Biomedical Engineering, Case Western Reserve University, Cleveland, OH, USA; and the Advanced Platform Technology Center, Louis Stokes Cleveland VA Medical Center, Cleveland, OH, USA. Quinn is with the Department of Mechanical and Aerospace Engineering, Case Western Reserve University, Cleveland, OH, USA. Hnat (sandra.hnat@case.edu) is corresponding author.

Controllers for balance are a topic of ongoing research in the robotics field, especially for anthropomorphic walking robots.[23] Recent advances in self-stabilizing controllers allow bipedal robots to walk across a variety of different terrains and perform tasks such as carrying boxes or opening doors.[24] Because of the commonality of the problem, these balance controllers for bipedal robots might be applicable to walking exoskeletons.

Various methods have been proposed to control the balance of bipedal robots, most notably the zero moment point, which is a projected point on the ground where the sum of the moments acting on the robot equal 0.[25,26] The zero moment point is equivalent to the center of pressure during standing and slow walking,[27] and during fast walking can be calculated based on the mediolateral (ML) and anteroposterior (AP) center of mass (COM) trajectories.[28] Many bipedal robots, particularly Honda's ASIMO robot (Honda Motor Company, Tokyo, Japan), have used zero moment point for standing and walking balance control,[29–32] and therefore require accurate measurements of COM as feedback.

Other balance controllers expand upon the concept of zero moment point, such as the centroidal moment pivot proposed by Herr et al.[33] This is a reference point that maintains a constant whole-body angular momentum, where stability is based on the separation between the centroidal moment pivot and the zero moment point. Another balance metric is the foot rotation indicator first proposed by Goswami,[34] which uses the stance-foot's angular acceleration as a measure of stability and has been used in conjunction with the zero moment point.[35] Other methods such as capture point[36] ensure the robot's feet are placed within a stability region influenced by the center of pressure.

These balance control strategies require a global, whole-body parameter to determine instances when the robot becomes unstable, such as when the next footstep would fall outside of the calculated stable region of support. These global balance parameters are fed back to the controllers to adjust the motor output needed to

maintain stability. Therefore, estimating them in real time is a critical component when designing a balance controller.

In robotics applications, COM can be estimated through dynamics and parameter identification of the biped, where information such as limb masses, inertias, and torques are easily measured.[37] However, this information is challenging to accurately measure when a human is introduced into the system. Instead, accurate measurements of COM kinematics can be obtained from optical motion capture systems,[38] which are limited to dedicated laboratories and unsuitable for devices designed for community use. Alternatively, inertial measurement units (IMUs) are becoming an increasingly popular tool for estimating gait kinematics due to their portability and low cost.[39] Joint trajectories can be estimated from body-worn IMUs during walking[40–42] and rehabilitative gait studies.[43,44] COM kinematics, some of the global balance parameters needed for robotic controller, can be estimated from commercial IMU systems in real time.[45–47]

Commercial IMU sensor systems require extensive calibration procedures to determine the orientation of each sensor with respect to each other and to each body segment. As IMU sensor calibrations usually require subjects to stand, sit, and walk within a specific time window,[40] these systems are not suited for subjects with SCI. Guo and Xiong[46] found that commercial IMU systems can produce large measurement errors when determining the location of the base of support, which is related to the COM, during dynamic movements while standing and even the optimal calibration motions they propose are too complex for individuals with SCI to perform.

Betker et al[38] estimated COM via a neural network, fuzzy logic, and genetic sum-of-sines with a relative error of 9.4% (0.9%) compared with motion capture from only 2 accelerometers (on the trunk and shank) while subjects moved their trunks sinusoidally in the AP direction. However, AP sinusoidal motions may not reflect real-world conditions or adequately capture information in the ML direction.

The purpose of this study is to explore whether whole-body COM kinematics can be predicted through an artificial neural network using acceleration signals obtained from a sensor array typical for powered exoskeletons. Here, we investigate if an artificial neural network can be trained to learn the relationship between COM displacement, as measured by gold-standard motion capture methods, and the corresponding changes in their accelerations measured by accelerometers. Throughout, we employ the standing motions and balance corrections from destabilized able-bodied participants, which reflect the limited ranges of motion and mechanical degrees of freedom exhibited by individuals with SCI wearing an exoskeleton while standing.

Methods

Standing Destabilization Experiments

We collected standing data from 5 able-bodied individuals (4 men and 1 woman; median age = 23; median height = 1.71 m, median weight = 61.7 kg). The study was approved by the institutional review board of the Louis Stokes Cleveland Veterans Affairs Medical Center (number 2008-027). Written informed consent was obtained from all participants.

Participants stood upright with feet apart within the work volume of a 16-camera motion-capture system (Vicon; Oxford Metrics, Oxford, United Kingdom) while holding handles instrumented with 6-axis load cells (MCW-500; Advanced Mechanical Technology Inc, Watertown, MA) attached to a custom aluminum standing frame to simulate standing after SCI, which requires a walker or assistive device to maintain balance and posture. The handles were 120-mm long and 25 mm in diameter, located approximately 1 m from the ground and 0.7 m apart. Load cell data was collected at 1000 Hz.

A total of 10 wireless triaxial accelerometers (Delsys; Trigno Wireless, Natick, MA) were affixed to the chest (2), sternum, navel, pelvis (2), each anterior thigh, and each anterior shank (Figure 1). Then, the 38 retroreflective markers of the Vicon's Plug-in Gait marker set were affixed, along with 10 additional markers on the accelerometers to record their locations on the participant. Motion capture data and accelerometer signals were collected at 100 and 1000 Hz, respectively.

The COM kinematics were calculated from motion capture and the regression equations of the U.S. Army anthropometric studies.[48] These equations provide the segmental mass parameters as functions of participant height and weight. A weighted average of the computed COM locations for each limb segment yielded the whole-body COM to be used as the gold standard for training the artificial neural network.

Subjects participated in 2 separate data collection sessions, each with a different set of perturbations paradigms. The first included unexpected, externally applied perturbations, while the second consisted of volitional, internally generated perturbations. These perturbations represented disturbances expected for a user wearing an exoskeleton: (1) external perturbations simulated destabilizing bumps or nudges and (2) internal perturbations represented disturbances from volitional movements simulating activities of daily living such as acquiring and repositioning

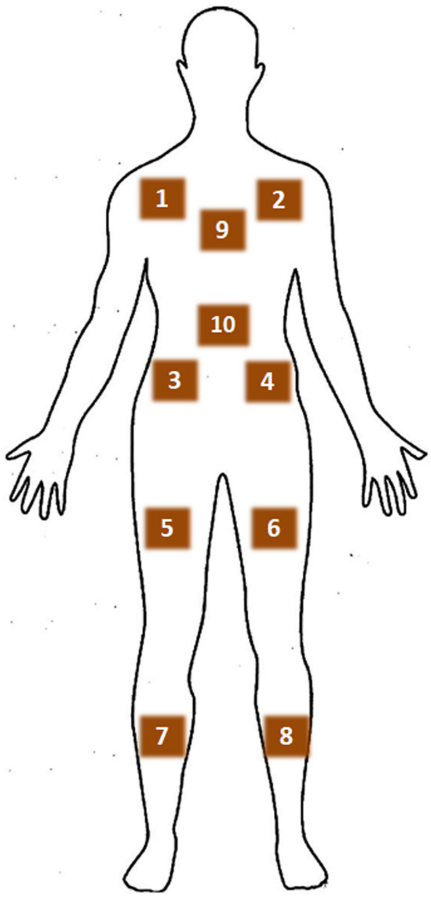

Figure 1 — Location of the 10 triaxial accelerometers mounted on the torso, sternum, navel, pelvis, anterior thighs, and anterior shanks.

objects. While COM can be estimated from larger motions, such as excessive trunk flexion[38] or motions like squatting,[46] the experimental protocol was designed to be applicable for users with SCI who may have limited ranges of motion and mechanical degrees of freedom during standing.

External Perturbations. There were 4 linear actuators (Copley Motion Control, Canton, MA) positioned at waist height immediately to the front, rear, left, and right of the participants that exerted controlled and repeatable, square force pulses lasting 500 millisecond in the AP and ML directions (Figure 2, left). Ropes from each actuator were attached to a harness secured to the waist to apply the perturbations to the pelvic region. Actuators were controlled by issuing a force command (expressed as a percentage of bodyweight, BW), which was converted to a control current sent to the actuators via a CAN connection from xPC Target toolbox in MATLAB™ Simulink™,® (MathWorks, Natick, MA).

Because the study focused on standing with a static base of support (the area of the support surface defined by the positions of the unmoving feet), small perturbations in each direction were prescribed at the start of each session that were discretely increased in magnitude throughout a series of separate trials until one or more of the following conditions were met: The participant (1) reported feeling uncomfortable by the perturbation magnitude, (2) stood on their toes, or (3) initiated or nearly initiated a step to restabilize. We then created 3 different perturbation magnitudes for each direction for a total of 12 different external perturbations per participant:

1. Large: the maximum tolerated perturbation, without taking a step
2. Small: 50% of the large perturbation
3. Medium: 75% of the large perturbation

The perturbation magnitudes for the 5 participants ranged between 5% and 20% BW, depending on their individual preferences. The largest tolerable magnitude consistently occurred in the forward direction (between 10% and 20%), while the smallest were in the backward direction (between 4% and 6%). After SCI, the maximum tolerated perturbation is likely to fall nearer the lower range of these magnitudes, and the protocol would need to be repeated to ensure safety of paralyzed volunteers.

Based on previous research for applying external perturbations to individuals with SCI,[49] we performed 20 repetitions per perturbation magnitude and direction for a total of 240 perturbations per participant. We separated the 240 perturbations into 10 trials containing 24 perturbations each, which were randomly assigned into separate trials using a MATLAB script.

Internal Perturbations. Participants moved 3 loaded jars back-and-forth between a central position and 4 different target locations on a wire rack (up, left, right, and down) using their right hand (Figure 2, right) for a total of 12 internal perturbations. Each movement cycle included

1. Standing stationary with both hands on the instrumented walker handles
2. Moving a specific jar to the target location read aloud by the investigator
3. Briefly removing the hand from the jar
4. Moving the jar back to the "home" location
5. Returning the hand back to the instrumented walker handle

We selected this protocol to easily determine the start and end times of each movement cycle performed at a self-selected pace. For instance, after lifting a hand off the walker handle to reach for a jar, the change in handle-force marked the start of the perturbation cycle. We chose the weight of the light, medium, and heavy jars based on the participants' comfortable range within 3% to 10% of their BW. The shelf racks were adjusted until the participants did not lift their feet off the force plates to complete any movement. The jars' "home" locations were on the centermost shelf, positioned at approximately 90° shoulder flexion with the heaviest jar on the left, the medium jar in the middle, and the lightest jar on the right.

Based on previous research using internal perturbations to destabilize individuals with SCI,[50] we selected 10 trials of 30 load transfers each for a total of 300 perturbations. The jar weight and target location were randomly assigned into separate trials using a MATLAB script.

COM Estimation Algorithm

Inputs to the artificial neural network trained to predict COM kinematics were the acceleration signals measured by the accelerometers, while the outputs were COM displacements in the AP and ML directions obtained through motion capture (Figure 3).

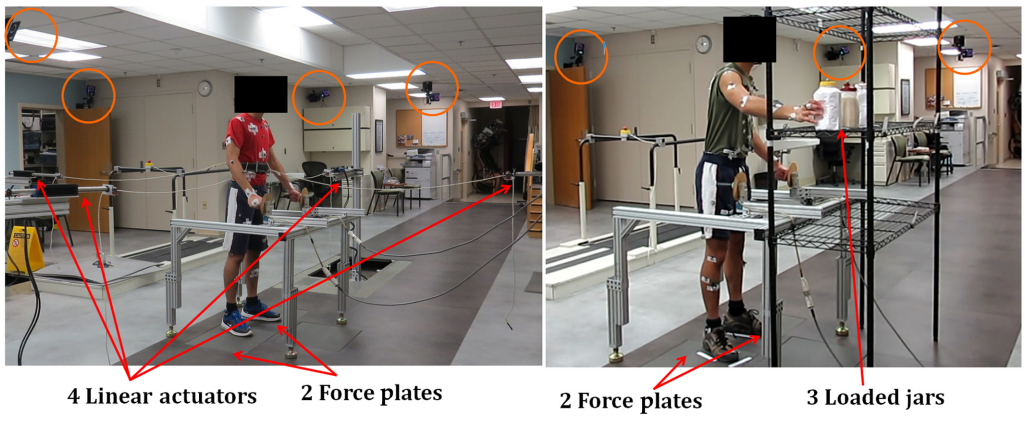

Figure 2 — Experimental setup with 48 reflective markers and ten triaxial accelerometers. Participants placed each foot on force plates and held the handles of an instrumented walker within the volume of a motion-capture system. Standing balance was then destabilized by either (left) unexpected perturbations caused by 4 linear actuators that pulled the participant in the forward, right, backward, and left directions, or (right) internal perturbations caused by volitionally moving 3 jars of different weights between 4 different target locations on a shelf.

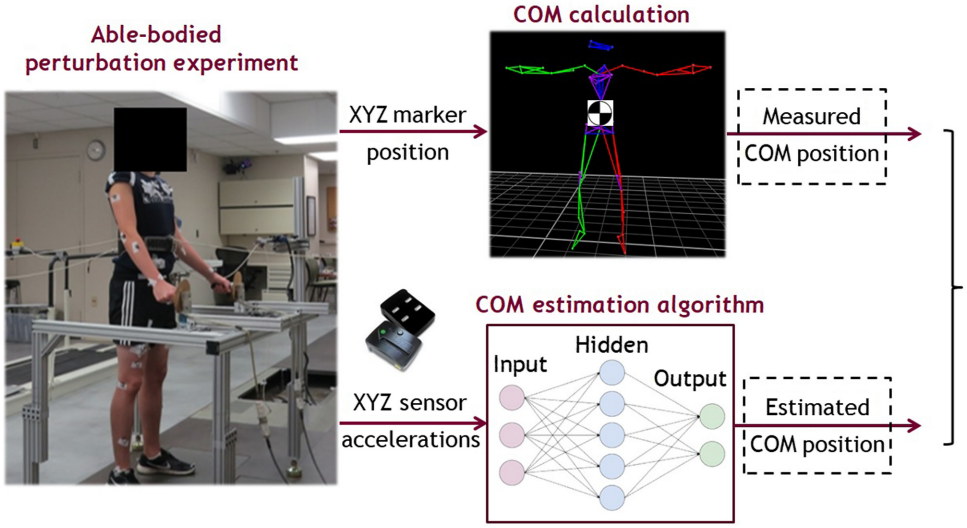

Figure 3 — Workflow for training an artificial neural network, where the inputs are XYZ accelerations measured from accelerometers and the outputs are the COM positions measured by motion capture. The ANN is trained by minimizing the mean squared error between the measured and estimated COM positions in the AP and ML directions. AP indicates anteroposterior; ANN, artificial neural network; COM, center of mass; ML, mediolateral.

Table 1 IP and EP Types Classifications

IP	EP
Jar A (heavy) Top (A1), left (A2), right (A3), bottom (A4)	Small Front (S0), right (S1), back (S2), left (S3)
Jar B (medium) Top (B1), left (B2), right (B3), bottom (B4)	Medium Front (M0), right (M1), back (M2), left (M3)
Jar C (light) Top (C1), left (C2), right (C3), bottom (C4)	Large Front (L0), right (L1), back (L2), left (L3)

Abbreviations: EP, external perturbations; IP, internal perturbation. Types of IP and EP, classified by magnitude (jar weight or actuator pull magnitude) and direction (shelf location or pull direction).

This network had a single hidden layer of sigmoidal transfer functions and a linear function in the output layer. The network was trained with the Deep Learning Toolbox™ in MATLAB and the Levenberg–Marquardt algorithm[51–54] where we specified the same 85% and 15% of the data for training and validation, respectively. Performance was quantified by minimizing a mean squared error (MSE) objective function between the COM estimated from motion capture (COM_{meas}) and the COM predicted from the network (COM_{pred}) where n is the number of data points:

$$MSE = \frac{1}{n}\sum_{i=1}^{n}(COM_{meas} - COM_{pred})^2 \quad (1)$$

Several networks were trained with 15 to 65 neurons in the hidden layer to determine the ideal number of neurons to achieve the lowest root mean square errors (RMSEs), which was obtained by taking the square root of the MSE. All results herein will be reported as RMSE.

After obtaining the optimal number of neurons, we then performed a *k*-fold cross-validation.[55] Since *k* values from 5 to 10 have been shown to produce acceptable bias and variance,[56] we selected 10 as the value for *k*. Initial conditions were set to the same randomized values, and we shuffled into the 10 training groups by selecting different sets of 10 trials for validation data of each *k*-fold. We then calculated the average RMSE among the folds and computed the error as a percentage between each fold and the average RMSE. If the average RMSE among folds is similar, and the percentage of difference is small, then the data set was determined to be rich enough to train the artificial neural network without risk of underfitting the data.

Statistical Analysis

After training the model, we separated the validation data into 24 perturbation types (12 internal perturbations and 12 external perturbations; Table 1). The external perturbations were classified by the perturbation direction and magnitude, while the internal perturbations were separated by jar weight and target location. We then categorized the validation data into perturbation types and defined each occurrence of a specific perturbation into a cycle, determined by its start and stop times. After the validation data was categorized into cycles, we calculated the mean and SD of the measured and predicted COM displacements during each perturbation type to define RMSE and the coefficient of determination, R^2, between COM_{meas} and COM_{pred}. The R^2 was calculated by dividing the sum of the residuals by the sum of squares, where COM_{meas} is the mean of the COM measured from motion capture:

$$R^2 = 1 - \left[\frac{\sum_i (COM_{meas} - COM_{pred})^2}{\sum_i (COM_{meas} - \overline{COM}_{meas})^2}\right] \quad (2)$$

The RMSE and the R^2 for each perturbation type determined how well the artificial neural network predicted the reactive COM displacements in response to specific perturbations, magnitudes, and directions.

Results

Prior to performing the analyses, we qualitatively determined that all subjects responded similarly to the prescribed perturbations, and no reactive responses differed enough from each other to exclude from the study.

A total of 50 neurons resulted in the best performance with an RMSE of 0.88 cm. Networks with more than 50 neurons produced higher errors, thereby overfitting the data. The results of the cross-validations produced an average RMSE of 1.12 cm, with errors ranging between 0.37% and 14.0% between the folds and this average. As the largest RMSE of 14% only yielded a 1.6-mm difference from the average, we determined that the experimental data were sufficient for training the artificial neural network.

Estimates from the artificial neural network on 60 seconds of validation data from an external perturbation trial (Figure 4) compared favorably to the COM displacement measured experimentally. In this representative data set, the predicted COM displacement showed a similar trend to the measured data and reached the peak magnitude in the AP direction (top), while the largest fitment errors occur at the peak ML displacements (bottom).

The averaged COM trajectories across all subjects for the specific movement types are shown (Figure 5). The COM in the sagittal and coronal planes correspond intuitively to the specific movement task. For instance, moving the jars to the second position on the shelf caused the participant to move to the left. The COM predominantly moved in the ML direction during the internal perturbations (left), with maximum distances from the origin of 7.4 and 3.53 cm for ML and AP, respectively. During the external perturbations (right), participants predominantly moved in the AP direction, with maximum displacements of 6.5 and 2.8 cm in the AP and ML directions, respectively.

The R^2 and RMSE of each perturbation type and COM direction are summarized in Table 2. Note that in the external perturbation data, some results are omitted because the participants were pulled by a single actuator in one direction. For instance, if the front actuator pulled the participant forward, their COM displacement was exclusively in the sagittal plane and fitment in the coronal plane was expected to be poor.

Throughout all trials, the average R^2 was .83 with 89% of the movements with an R^2 larger than .70, suggesting a strong relationship between the measured and predicted COM displacements.[57] Overall, the algorithm better predicts movements in the ML direction for both the external perturbations and internal perturbations, with an average R^2 of .88 and .92, respectively. In the AP direction, the average R^2 is .80 for the external perturbations, and .75 for the internal perturbations.

Across all trials, the mean RMSE was .59 cm, with the largest errors of 1.81 cm (L2, AP) and 1.01 cm (L3, ML), suggesting that the algorithm struggles to reach the maximum displacement in the largest external perturbations. The RMSE increased with perturbation magnitude, with average errors of 14.6% and 22.0% in the AP and ML directions, respectively. These errors translate to 0.94 cm in the sagittal plane and 0.60 cm in the coronal plane. During the internal perturbations, there appeared to be no relationship between the RMSE and the jar weight or target location on the shelf. The average errors for the internal perturbations were 7.3% and 12.9% in the ML and AP directions, respectively, which correspond to approximately 0.5-cm COM displacement error in both planes.

To better visualize the results, the averaged movement cycles in the ML direction during the internal perturbations are shown (Figure 6), where the R^2 between the measured COM and the predicted COM is indicated, along with the perturbation type. Translucent, shaded regions indicate one SD away from the mean.

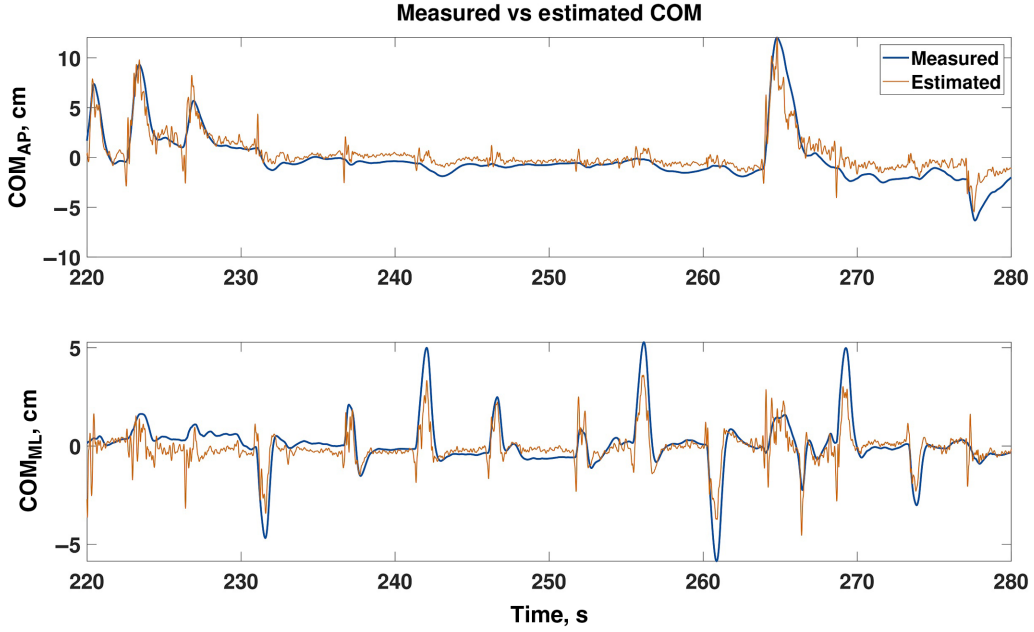

Figure 4 — COM displacements measured experimentally from motion capture (thick) and estimated through the COM estimation algorithm (thin) during an external perturbation trial. The data presented here are part of the validation data set. Only 60 seconds of the trial are shown. AP indicates anteroposterior; COM, center of mass; ML, mediolateral.

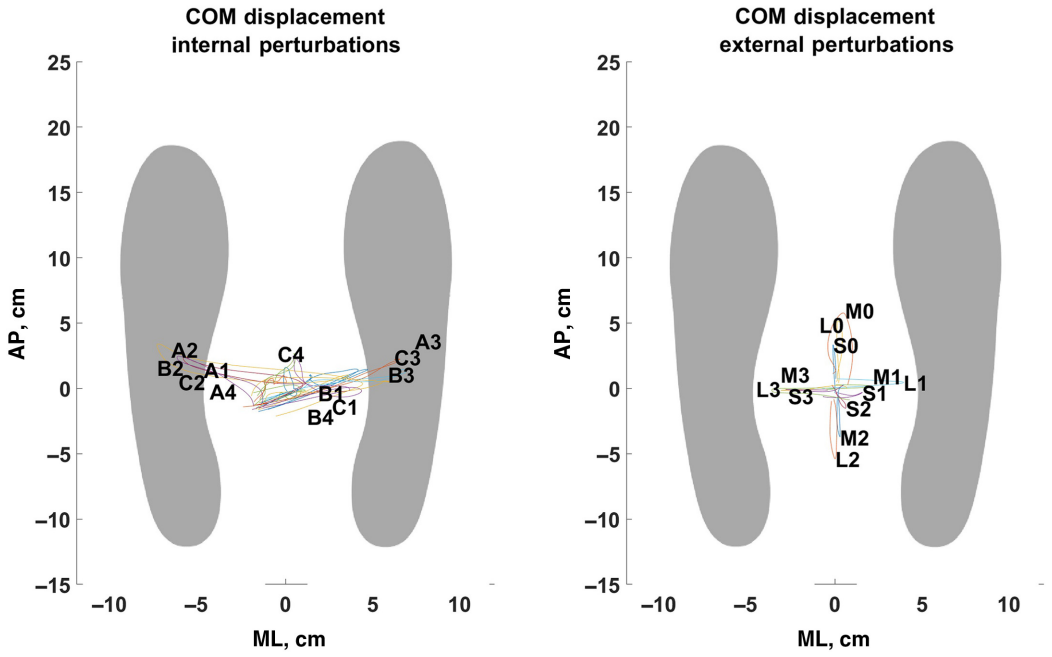

Figure 5 — Averaged COM movement per perturbation type during internal perturbations (left) and external perturbations (right). The perturbation type for each movement is indicated at the maximum distance away from the origin, in between the participants' feet. To better visualize how far the COM was displaced from the starting position, we included a shoeprint to approximate the foot position, which were determined by taking the average position of toe, heel, and lateral ankle markers throughout the trials. Refer to Table 1 for the notations used in the figure. AP indicates anteroposterior; COM, center of mass; ML, mediolateral.

Discussion

We presented a method of calculating whole-body COM kinematics to be used as global feedback parameters for standing balance controllers. Although commercially available motion capture systems[38] and IMU systems are able to estimate COM kinematics[40] in real time, the presented algorithm is based on easily-mounted accelerometers suitable for integrating into exoskeletal systems for community use. Such a strategy is necessary for standing and walking stability of exoskeletons for individuals with an SCI.

Through able-bodied perturbed standing experiments, the algorithm's predicted COM kinematics strongly described the majority of observed COM displacements in the AP and ML directions measured by a motion capture system. Based on the low average error (RMSE < 1.0 cm) and large average R^2 of .83, the algorithm can replicate the majority of COM displacements induced by the prescribed unexpected and volitional destabilizing movements. Previous studies found that commercial IMU systems produce large measurement errors between −12.6% and +64.6% when determining the location of the base of support, related to the COM, during dynamic movements,[46] whereas our algorithm's RMSE error fell within 7.3% to 22.0%. This compares favorably to Betker et al[38] (9.4% [0.9%]) from stereotypical rhythmic sinusoidal motions exclusively in the AP direction.

The largest errors occurred when predicting peak displacements, with RMSE values ranging between .5 and 1.0 cm. In bipedal walking robots, the COM or the center of pressure obtained from mathematical models describing the biped are inexact, but balance controllers can be effective despite these approximations as long as they are kept within the size range of a humanoid foot.[36] We expect that the errors of 1 cm estimated from our algorithm could be accounted for by a robust balance controller.

Intuitively, an algorithm based on an artificial neural network will prioritize minimizing the error during the instances of the largest COM displacements, which would occur in the AP direction for external perturbations, and the ML direction for internal perturbations. As an example, the R^2 for moving jar B to position 1 is .18 in the AP direction but .87 in the ML direction. This directly corresponds to the amount of COM movement observed in the coronal and sagittal planes for this perturbation type. Lower R^2 values may not necessarily indicate that the algorithm performs poorly during these instances but could be explained by less movement during those tasks in the specified direction. Alternatively, participants may not be consistently responding to the perturbations, within or between trials, or among each other. As some variability exists between participants, the algorithm would struggle to predict these instances if no clear pattern emerges during the specific movement.

Within the selected validation data, it is important to note that the medium external perturbation in the forward direction (M0) caused the participants to move farther forward than the pulls induced by the largest magnitude (L0). This is a feature of this specific sample of data used as part of the validation set where the participants may have reacted more strongly to the particular perturbation. As the perturbations are (1) randomized and (2) repeated multiple times throughout the trial, it is possible for identical perturbations to be prescribed in succession. In this case, participants may begin to anticipate and resist the perturbation, which would reduce their reactive COM displacement (as in the case of L0).

One study limitation is that the destabilizing movements prescribed throughout the experiments were not large enough for the participant to take a step in any direction or shift their

Table 2 Statistical Analysis for Perturbations, RMSE, and R^2

	AP		ML	
Perturbation	**R^2**	**RMSE, cm**	**R^2**	**RMSE, cm**
EPs				
Small				
S0	.87	.47	—	—
S1	—	—	.9	.24
S2	.55	.52	—	—
S3	—	—	.94	.39
Medium				
M0	.79	1.11	—	—
M1	—	—	.86	.43
M2	.92	.88	—	—
M3	—	—	.85	.72
Large				
L0	.88	.89	—	—
L1	—	—	.84	.91
L2	.77	1.81	—	—
L3	—	—	.87	1.01
Mean (SD)	.80 (.13)	.95 (.49)	.88 (.04)	.62 (.31)
IPs				
Jar A(heavy)				
A1	.86	.30	.96	.33
A2	.91	.42	.97	.54
A3	.81	.64	.97	.82
A4	.84	.48	.95	.35
Jar B(medium)				
B1	.18	.55	.87	.53
B2	.78	.33	.96	.58
B3	.86	.42	.97	.80
B4	.76	.44	.75	.33
Jar C(light)				
C1	.60	.41	.83	.47
C2	.69	.40	.96	.57
C3	.87	.51	.97	.78
C4	.80	.58	.85	.42
Mean (SD)	.75 (.20)	.46 (.10)	.92 (.07)	.54 (.18)

Abbreviations: AP, anteroposterior; EP, external perturbations; IP, internal perturbations; ML, mediolateral; RMSE, root mean square error. Note: RMSE and coefficient of determination R^2 for each perturbation type in the AP and ML directions.

weight onto their toes. Similarly, the protocol restricted the participants to hold onto the handles of the instrumented standing frame, which could counteract the prescribed perturbations. On average, the COM displacements in the AP direction during the external perturbations were less than half of the distance to the participants' base of support, with the maximum displacements stopping within the midfoot region before the metatarsophalangeal joint. While there are several important aspects of balance control that occur during, before, or after reactive steps, these investigations fall outside the scope of this work. The prescribed perturbations were enough for an artificial neural network to learn the relationship between COM displacement and acceleration signals measured by the accelerometers. For larger movements involving more degrees of freedom involving the legs or trunk, we expect that the algorithm would need to be retrained with different calibration data. These movements were excluded in the current study, which exclusively focused on standing motions that could be performed by an individual with SCI.

Another limitation of the current study is that knowledge of the COM in the inferior–superior direction and COM accelerations were not included in this analysis, although they are often used to calculate the zero moment point.[28] Acceleration signals alone cannot provide information about the COM's absolute vertical position in 3-D space, which is approximately the height from the ground to the individual's waist.

Throughout the trials and movement types, the average coefficient of determination was 0.83 with 89% of the movements with $R^2 > .70$, while the average RMSE errors ranged between 7.3% and

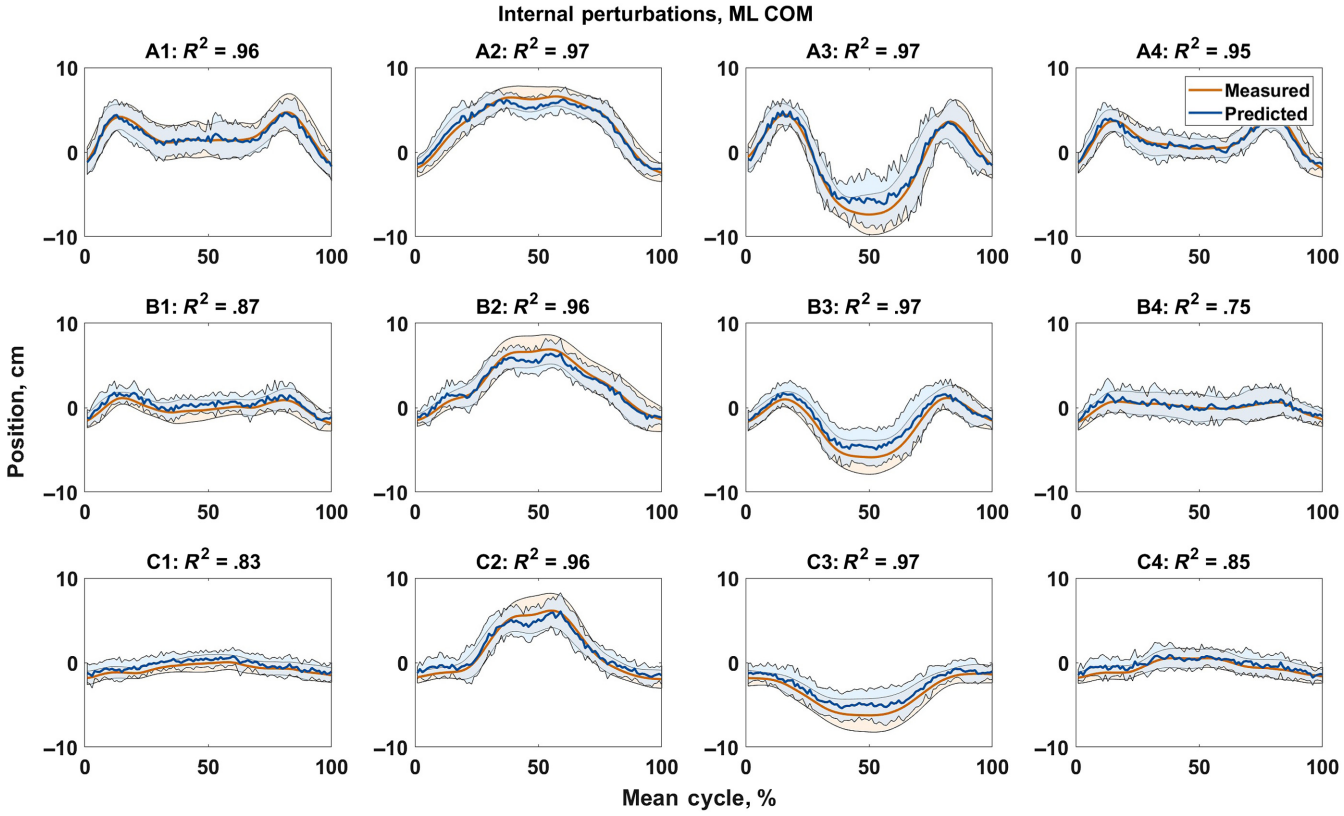

Figure 6 — Averaged COM displacements in the ML direction during internal perturbations, comparing the measured COM (thin) and the predicted COM (thick). Translucent, shaded regions correspond to one SD from the mean. The perturbations are classified by: (1) the jar weight of heavy (A), medium (B), and light (C), and (2) the target location on the shelf: top (1), left (2), right (3), and bottom (4). COM indicates center of mass; ML, mediolateral.

22.0% corresponding to 0.5 and 0.94 cm error in both the coronal and sagittal planes. This demonstrates that COM kinematics in the AP and ML direction can be estimated from only acceleration signals measured by accelerometers. Though our method is motivated by designing a standing balance controller for powered exoskeletons, the procedure is general and can be applied to other studies, such as gait studies where COM kinematics are measured, especially during activities outside of a gait lab.

Acknowledgments

This research is supported by grants from the National Science Foundation Cyber-Physical Systems Award Number 1739800 and the National Institutes of Health Grant: R01 NS040547-13, and also with the support of laboratory and other facilities located at the Advanced Platform Technology Center in the Louis Stokes Cleveland VA Medical Center, Cleveland, OH. The authors have no conflict of interest to disclose.

References

1. Stevens SL, Caputo JL, Fuller DK, Morgan DW. Physical activity and quality of life in adults with SCI. *J Spinal Cord Med*. 2008;31(4): 373–378. PubMed ID: 18959354 doi:10.1080/10790268.2008.11760739
2. SCI facts and injuries at a glance. https://www.nscisc.uab.edu/Public/Facts%20and%20Figures%202019%20-%20Final.pdf. Accessed February 25, 2020.
3. Jain NB, Ayers GD, Peterson EN, Harris MB, Morse L, O'Connor KC, Garshick E. Traumatic SCI in the United States, 1993–2012. *JAMA*. 2015;313:2236–2243. PubMed ID: 26057284
4. Lasfargues JE, Custis D, Morrone F, Carswell J, Nguyen T. A model for estimating SCI prevalence in the United States. *Spinal Cord*. 1995;33(2):62–68. doi:10.1038/sc.1995.16
5. Dollar AM, Herr H. Lower extremity exoskeletons and active orthoses: challenges and state-of-the-art. *IEEE Trans Rob*. 2008;24(1): 144–158. doi:10.1109/TRO.2008.915453.
6. Anam K, Al-Jumaily AA. Active exoskeleton control systems: state of the art. *Procedia Eng*. 2012;41:988–994. doi:10.1016/j.proeng.2012.07.273
7. Díaz I, Gil JJ, Sánchez E. Lower-limb robotic rehabilitation: literature review and challenges. *J Robot*. 2011;2011:1–11. doi:10.1155/2011/759764
8. Winfree KN, Stegall P, Agrawal SK. Design of a minimally constraining, passively supported gait training exoskeleton: ALEX II. 2011 IEEE International Conference on Rehabilitation Robotics; 2011:1–6.
9. Banala SK, Agrawal SK, Scholz JP. Active Leg Exoskeleton (ALEX) for gait rehabilitation of motor-impaired patients. 2007 IEEE 10th International Conference on Rehabilitation Robotics; 2007:401–407
10. Veneman JF, Kruidhof R, Hekman EEG, Ekkelenkamp R, Asseldonk EHF, Van der Kooij H. Design and evaluation of the LOPES exoskeleton robot for interactive gait rehabilitation. *IEEE Trans. Neural Syst Rehabil Eng*. 2007;15(3):379–386. PubMed ID: 17894270 doi:10.1109/TNSRE.2007.903919

11. What's HAL? – The World's First Cyborg Type Robot. https://www.cyberdyne.jp/english/products/HAL/. Accessed February 25, 2020.
12. Kolakowsky-Hayner SA, Crew J, Moran S, Shah A. Safety and feasibility of using the Ekso bionic exoskeleton to aid ambulation after SCI. *J Spine*. 2013;4:1–8.
13. ReWalk – More than Walking http://rewalk.com. Accessed February 25, 2020.
14. Parker Indego. http://www.indego.com/indego/en/home. Accessed February 25, 2020.
15. Kawamoto H, Lee S, Kanbe S, Sankai Y. Power assist method for HAL-3 using EMG-based feedback controller. *IEEE Int Conf Syst Man Cyber*. 2003;2:1648–1653.
16. Esquenazi A, Talaty M, Packel A, Saulino M. The ReWalk powered exoskeleton to restore ambulatory function to individuals with thoracic-level motor-complete SCI. *Am J Phys Med Rehabil*. 2012;91(11):911–921. PubMed ID: 23085703 doi:10.1097/PHM.0b013e318269d9a3
17. Esquenazi A. New bipedal locomotion options for individuals with thoracic level motor complete SCI. *J Spinal Res Found*. 2013;8:26–28
18. Farris RJ, Quintero HA, Murray SA, Ha KH, Hartigan C, Goldfarb M. A preliminary assessment of legged mobility provided by a lower limb exoskeleton for persons with paraplegia. *IEEE Trans Neural Syst Rehabil Eng*. 2014;22(3):482–490. PubMed ID: 23797285 doi:10.1007/978-3-319-08072-7_38
19. Veneman JF. Exoskeletons supporting postural balance–the BALANCE project. *Replace, Repair, Restore, Relieve–Bridging Clinical and Engineering Solutions in Neurorehabilitation*. Springer International Publishing, Cham, Switzerland. 2014;203–208. doi:10.1109/TNSRE.2013.2268320
20. Miller LE, Zimmermann AK, Herbert WIG. Clinical effectiveness and safety of powered exoskeleton-assisted walking in patients with SCI: systematic review with meta-analysis. *Med Dev Evid Res*. 2016;9:455. doi:10.2147/MDER.S103102
21. Evans N, Hartigan C, Kandilakis C, Pharo E, Clesson I. Acute cardiorespiratory and metabolic responses during exoskeleton-assisted walking overground among persons with chronic SCI. *Top SCI Rehab*. 2015;21:122–132.
22. Asselin P, Knezevic S, Kornfeld S, Cirnigliaro C, Agranova-Breyter I, Bauman WA, Spungen AM. Heart rate and oxygen demand of powered exoskeleton-assisted walking in persons with paraplegia. *J Rehab Res Develop*. 2015;52(2):147–158. PubMed ID: 26230182 doi:10.1682/JRRD.2014.02.0060.
23. Katic D, Vukobratovic M. Survey of intelligent control techniques for humanoid robots. *J Intell Rob Syst*. 2003;37:117–141.
24. Kuindersma S, Deits R, Fallon M, et al. Optimization-based locomotion planning, estimation, and control design for Atlas. *Auton Robots*. 2016;40(3):–455. doi:10.1007/s10514-015-9479-3
25. Vukobratovic M, Juricic D. Contribution to the synthesis of biped gait. *IEEE Trans Biomed Eng*. 1969;BME(1):1–6. doi:10.1109/TBME.1969.4502596
26. Vukobratovic M, Borovac B. Zero-moment point—thirty five years of its life. *Int J Humanoid Rob*. 2004;1:157–173.
27. Sardain P, Bessonnet G. Forces acting on a biped robot: center of pressure—zero moment point. *IEEE Trans Syst Man Cyber Part A Syst Hum*. 2004;34(5):630–637. doi:10.1109/TSMCA.2004.832811
28. Kim J-Y, Park I-W, Oh J-H. Experimental realization of dynamic walking of the biped humanoid robot KHR-2 using zero moment point feedback and inertial measurement. *Adv Rob*. 2006;20(6):707–736. doi:10.1163/156855306777361622.
29. Hirose M, Ogawa K. Honda humanoid robots development. *Philosoph Trans R Soci A Math Phys Eng Sci*. 2007;365(1850):11–19. doi:10.1098/rsta.2006.1917
30. Takenaka T, Matsumoto T, Yoshiike T. Real time motion generation and control for biped robot 1st report: walking gait pattern generation. 2009 IEEE/RSJ International Conference on Intelligent Robots and Systems, St. Louis, MO, USA. 10841091IEEE 2009.
31. Takenaka T, Matsumoto T, Yoshiike T, Shirokura S. Real time motion generation and control for biped robot -2nd report: Running gait pattern generation. 2009 IEEE/RSJ International Conference on Intelligent Robots and Systems; 2009. St. Louis, MO. 1092-1099IEEE.
32. Takenaka T, Matsumoto T, Yoshiike T, Hasegawa T, Shirokura S, Kaneko H, Orita A. Real time motion generation and control for biped robot -4th report: Integrated balance control. 2009 IEEE/RSJ International Conference on Intelligent Robots and Systems; 2009. St. Louis, MO.1601-1608IEEE.
33. Herr HA, Popovic M. New horizons for orthotic and prosthetic technology: merging body and machine. ZIF International Conference on Walking Machines; 2003. Bielefeld, Germany.
34. Goswami A. Postural stability of biped robots and the foot rotation indicator (FRI) point. *Int J Rob Res*. 1999;18(6):523–533. doi:10.1177/02783649922066376.
35. Popovic MB, Goswami A, Herr H. Ground reference points in legged locomotion: definitions, biological trajectories and control implications. *Int J Rob Res*. 2005;24(12):1013–1032. doi:10.1177/0278364905058363.
36. Pratt J, Carff J, Drakunov S, Goswami A. Capture point: a step toward humanoid push recovery. 2006 6th IEEE-RAS International Conference on Humanoid Robots; 2006. Genova, Italy: University of Genova: 200-207.
37. Khosla PK, Kanade T. Parameter identification of robot dynamics. 24th IEEE Conference on Decision and Control; 1985, December. Fort Lauderdale, FL.
38. Betker AL, Moussavi ZMK, Szturm T. Center of mass approximation and prediction as a function of body acceleration. *IEEE Trans Biomed Eng*. 2006;53(4):686–693. PubMed ID: 16602575 doi:10.1109/TBME.2006.870222.
39. Cuesta-Vargas AI, Galán-Mercant A, Williams JM. The use of inertial sensors system for human motion analysis. *Phys Ther Rev*. 2010;15(6):462–473. PubMed ID: 23565045 doi:10.1179/1743288X11Y.0000000006.
40. Roetenberg D, Luinge H, Slycke P. Xsens MVN: Full 6DOF human motion tracking using miniature inertial sensors. *Xsens Motion Technol BV Tech. Rep. 1*. 2009;3.
41. Gil-Agudo A, Los Reyes-Guzman A, Dimbwadyo-Terrer I, et al. A novel motion tracking system for evaluation of functional rehabilitation of the upper limbs. *Neural Regen Res*. 2013;8:1773–1782. PubMed ID: 25206474
42. Findlow A, Goulermas JY, Nester C, Howard D, Kenney LPJ. Predicting lower limb joint kinematics using wearable motion sensors. *Gait & Posture*. 2008;28(1):120–126. PubMed ID: 18093834 doi:10.1016/j.gaitpost.2007.11.001
43. Cutti AG, Ferrari A, Garofalo P, Raggi M, Cappello A, Ferrari A. 'Outwalk': a protocol for clinical gait analysis based on inertial and magnetic sensors. *Med Biol Eng Comput*. 2010;48(1):17–25. PubMed ID: 19911214 doi:10.1007/s11517-009-0545-x
44. Vries SI, Bakker I, Hopman-Rock M, Hirasing RA, Mechelen W. Clinimetric review of motion sensors in children and adolescents. *J Clin Epidemiol*. 2006;59(7):670–680. PubMed ID: 16765269 doi:10.1016/j.jclinepi.2005.11.020
45. Esser P, Dawes H, Collett J, Howells K. IMU: Inertial sensing of vertical CoM movement *J Biomech*. 2009;42(10):1578–1581. PubMed ID: 19442978 doi:10.1016/j.jbiomech.2009.03.049
46. Guo L, Xiong S. Accuracy of base of support using an inertial sensor based motion capture system. *Sensors*. 2017;17(9):2091. doi:10.3390/s17092091

47. Fuschillo VL, Bagala F, Chiari L, Cappello A. Accelerometry-based prediction of movement dynamics for balance monitoring. *Med Biol Eng Comput*. 2012;50(9):925–936. PubMed ID: 22802142 doi:10.1007/s11517-012-0940-6
48. McConville JT, Clauser CE, Churchill TD, Cuzzi JR, Kaleps I. *Anthropometric relationships of body and body segment moments of inertia in AFAMRL-TR-80-119*. Ohio: U.S. Air Force Aerospace Medical Research Laboratory, Wright-Patterson Air Force Base; 1980.
49. Nataraj R, Audu M, Triolo RJ. Center of mass acceleration feedback control of standing balance by functional neuromuscular stimulation against external postural perturbations. *IEEE Trans Biomed Eng,* 2012;60(1):10–19. PubMed ID: 22987499 doi:10.1109/TBME.2012.2218601
50. Nataraj R, Audu M, Triolo RJ. Center of mass acceleration feedback control of functional neuromuscular stimulation for standing in the presence of internal postural perturbations. *J Rehab Res Develop*. 2012;49(6):889. PubMed ID: 23299260 doi:10.1682/JRRD.2011.07.0127
51. Levenberg K. A method for the solution of certain non-linear problems in least squares. *Q Appl Math*. 1944;2(2):164–168. doi:10.1090/qam/10666
52. Marquardt DW. An algorithm for least-squares estimation of nonlinear parameters. *J Soci Indus Appl Math*. (1963); 11(2): 431–441. doi:10.1137/0111030
53. Hagan MT, Menhaj M. Training feed-forward networks with the Marquardt algorithm. *IEEE Trans Neural Netw*. 1994;5(6):989–993. PubMed ID: 18267874 doi:10.1109/72.329697
54. Hagan MT, Demuth HB, Beale MH. *Neural Network Design,* Boston, MA: PWS Publishing; 1996.
55. Hastie T, Tibshirani R, Friedman J. *The Elements of Statistical Learning: Data Mining, Inference, and Prediction*. Springer Science & Business Media; 2009.
56. James G, Witten D, Hastie T, Tibshirani R. *An Introduction to Statistical Learning: with Applications in R;117*. New York, NY: Springer; 2013.
57. Moore NWI, Flinger MA. *The Basic Practice of Statistics*. 6th ed. New York, NY: Freeman and Company; 2013.